JOURNAL OF APPLIED PHYSICS 119, 135705 (2016)

Photo-electrical and transport properties of hydrothermal ZnO

P. Onufrijevs,[1,a)] P. Ščajev,[2] K. Jarašiūnas,[3] A. Medvid,[1] V. Korsaks,[4] N. Mironova-Ulmane,[4] M. Zubkins,[4] and H. Mimura[5]

[1]*Institute of Technical Physics, Faculty of Materials Science and Applied Chemistry, Riga Technical University, 3/7 Paula Valdena Str., LV-1048 Riga, Latvia*
[2]*Institute of Applied Research, Vilnius University, Sauletekio Ave. 3, Vilnius 10222, Lithuania*
[3]*Department of Semiconductor Physics, Vilnius University, Sauletekio Ave. 3, Vilnius 10222, Lithuania*
[4]*Institute of Solid State Physics, University of Latvia, 8 Kengaraga Str., 1063 Riga, Latvia*
[5]*Research Institute of Electronics, Shizuoka University, 3-5-1 Johoku, Naka-ku, Hamamatsu 432-8011, Japan*

(Received 7 January 2016; accepted 17 March 2016; published online 4 April 2016)

We performed the studies of optical, photoelectric, and transport properties of a hydrothermal bulk n-type ZnO crystal by using the contactless optical techniques: photoluminescence, light-induced transient grating, and differential reflectivity. Optical studies revealed bound exciton and defect-related transitions between the donor states (at $\sim$60 meV and $\sim$240 meV below the conduction band) and the deep acceptor states (at 0.52 eV above the valence band). The acceptor state was ascribed to V_{Zn}, and its thermal activation energy of 0.43 eV was determined. A low value of carrier diffusion coefficient ($\sim$0.1 cm^2/s) at low excitations and temperatures up to 800 K was attributed to impact the recharged deep acceptors. Electron and hole mobilities of 140 and $\sim$80 cm^2/Vs, correspondently, were determined at room temperature. The decrease of carrier lifetime with excitation was ascribed to increasing rate of radiative recombination at low temperatures and nonradiative recombination above the room temperature. © *2016 AIP Publishing LLC*.
[http://dx.doi.org/10.1063/1.4945016]

I. INTRODUCTION

ZnO has attracted quite much attention due to its unique optical, electrical, piezoelectric, magnetic properties.[1] Low cost of ZnO and its high exciton binding energy of $E_B = 60$ meV makes it a promising material for UV optoelectronics[2–4] and other applications.[5–8] Bulk ZnO crystals can be grown with a variety of techniques, including hydrothermal (HT) growth,[9] vapor-phase transport,[10] and pressurized melt growth.[11] Among them, the HT method is the most suitable for the growth of large-size crystals with high crystalline quality at relatively low temperatures and cost.[1] However, non-controllable impurities, such as Li and K, which are present in the solvent, usually have strong impact on the electrical and optical properties. For example, Li on a Zn site is a deep acceptor that compensates the n-type conductivity caused by other intrinsic impurities; therefore, HT ZnO bulk crystals are highly resistive (up to 380 Ω cm).[12] Also native defects such as Zn interstitials and vacancies[13] are abundant and strongly impact photoluminescence (PL) emission.

In this work, we report on optical and photo-electrical properties of the HT-grown ZnO bulk crystal. We applied complementary optical techniques of photoluminescence, differential reflectivity (DR), and light-induced transient grating (LITG) for investigation of carrier dynamics and determination of key photoelectrical and electrical parameters of bulk ZnO. The studies revealed strong impact of compensating defects, resulting in low carrier diffusion coefficient as well as deep defect governed, temperature- and excitation-dependent carrier lifetime. Radiative recombination rate at low temperatures provided radiative recombination coefficient.

II. SAMPLE AND EXPERIMENTAL TECHNIQUES

Commercial ZnO single crystal was purchased from Crystal Base Co. Ltd.[14] The size of the double-side polished crystal is 10.0 × 10.0 × 0.5 mm. The sample was grown by hydrothermal method in high pressure autoclaves by means of direct temperature drop in aqueous solutions of KOH and LiOH. High concentration of residual Li atoms in the range from 1×10^{17} to 5×10^{17} cm^{-3} (Ref. 15) and $\sim$5 ppm of Mg are typical values for this growth technology.[15] However, it must be noted that not all impurities would lead to the same electrically active defect levels as in ZnO different impurities have by order of magnitude different doping efficiencies.[16] The Li impurities can create shallow acceptor states at 120 meV (Ref. 17) or 150 meV (Refs. 18 and 19) above E_V, while Mg is an isovalent impurity (thus electrically inactive). The 120–150 meV acceptors are probably Li complexes,[20] as it is known that Li acceptors are much deeper: hybrid functional calculations[21,22] provide activation energy of $\sim$0.8 eV for substitutional Li_{Zn}. Experimental values are rather close: $\sim$0.86 eV.[23]

A. Sample electrical properties

Electrical parameters of the sample were determined using Ecopia Hall Effect Measurement System 5300. Four titanium contacts were deposited by DC magnetron sputtering in the corners of the square ZnO sample. A metallic titanium

a)Author to whom correspondence should be addressed. Electronic mail: onufrijevs@latnet.lv. Tel.: +37167089160. Fax: +37167089074. Present address: Pavels Onufrijevs at Research Laboratory of Semiconductor Physics, Institute of Technical Physics, Riga Technical University, 3/7 Paula Valdena Str., Riga LV-1048, Latvia.

 © 2016 AIP Publishing LLC

target was sputtered in an ambient of argon in a working pressure of 0.75 Pa. Four-probe conductivity measurements (Van der Pauw method) provided 17.1 Ω cm resistivity, residual electron concentration, $n_0 = 2.6 \times 10^{15}\,cm^{-3}$, and mobility $\mu_e = 140\,cm^2/V$ s at 300 K. Hall electron mobility value in the studied sample is lower than that for a weakly compensated ZnO, 220 cm^2/V s,[24] due to the ionized impurity scattering.

Measurements in 180–330 K temperature range provided electron concentration and Hall mobility temperature dependences (Fig. 1). The measured electron mobility μ_e in our case can be described by $1/\mu_e = 1/\mu_{latt} + 1/\mu_{II}$ equation, where μ_{latt} and μ_{II} are the lattice and the ionised impurity scattering mobilities, respectively. The μ_{latt} dependence is known as $235 \times (T[K]/300\,K)^{-1.9}$ cm^2/V s.[10] Fitting of the mobility dependence in the studied temperature range provided $\mu_{II} = 314 \times (T[K]/300\,K)^{3/2}$ cm^2/V s relationship.[25] Using equations of ionised impurity scattering mobility[25] and ZnO parameters,[26] we evaluated acceptor density as $N_A \sim 1.0 \times 10^{19}\,cm^{-3}$. Modeling of the n(T) dependence by equations from Ref. 10 provided the donor activation energies of 6 and 244 meV and concentrations of $1.00 \times 10^{19}\,cm^{-3}$ and $3.45 \times 10^{17}\,cm^{-3}$, respectively. The fitting of $n_0(T)$ directly by exponential function $\sim\exp(E_a/kT)$ (see Fig. 1) provided effective thermal activation energy of 110 meV.

B. Optical characterisation techniques

PL technique was used to measure emission spectra in wide temperature range (8–300 K) and identify the defect related features. Time-resolved pump-probe optical techniques of DR[27] and LITG[28] provided carrier lifetime, diffusion coefficient, and their dependences on temperature and excess carrier density. DR was used to monitor carrier density closer to the surface than LITG.

For PL measurements in backward configuration, we used 5 ns duration laser pulses at 263 nm. The excitation spot was $\sim$1 mm^2. The PL signal was analyzed using a monochromator and detected by a CCD camera in accumulation mode. Spectral resolution was $\sim$10 meV. The sample temperature was changed by placing the sample in a closed-cycle He cryostat. Excitation fluence was equal to

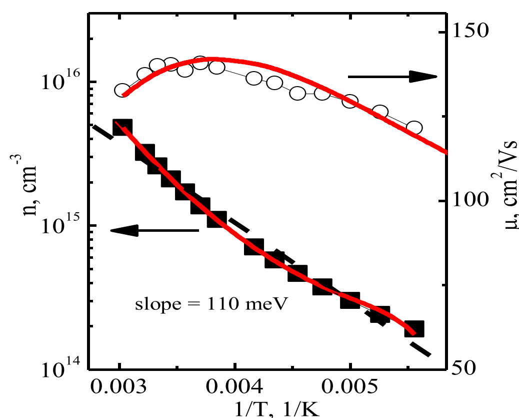

FIG. 1. Temperature dependences of electron concentration and mobility; solid lines show numerical fits, while dashed line is an exponential fit.

0.25 mJ/cm^2 ($P_0 = 50\,kW/cm^2$ peak power density). The excited carrier density of about $10^{18}\,cm^{-3}$ was estimated from the relationship $\Delta N \sim P_0\alpha_{ex}/2h\nu_{ex} \times \tau$, taking the measured excess carrier lifetime of $\tau \sim 200$ ps (will be given below).

DR and LITG measurements were performed by using 15 ps duration laser pulses at 355 nm wavelength ($h\nu_{ex} = 3.49$ eV). For measurements in the 80–800 K temperature range, a liquid nitrogen cryostat was used. The excitation fluence varied from $I_0 \approx 0.01$ mJ/cm^2 to $I_0 \approx 5$ mJ/cm^2, which generated the excess carrier (electron and hole) density $\Delta N_0 = \alpha_{ex} I_0/h\nu_{ex}$ from $\sim 10^{18}\,cm^{-3}$ up to $\sim 5 \times 10^{20}\,cm^{-3}$ at the excited surface (using the absorption coefficient value $\alpha_{ex} \sim 1.4 \times 10^5\,cm^{-1}$ (Ref. 29) at 355 nm). The photoexcited carriers were exponentially distributed within a layer of thickness $d_{ex} = 1/\alpha_{ex} \sim 70$ nm. An optically delayed (up to 4 ns) probe beam at $\lambda_p = 1064$ nm wavelength ($h\nu_{pr} = 1.17$ eV) was used to monitor the fast kinetics of induced DR and LITG decays.

Equation (1) provides the relationships between the measured DR and LITG signal values and excess carrier density ΔN. Change of sample reflectivity and its decay DR(t) after photoexcitation provided carrier lifetime in the vicinity of the surface (within the depth $d_{obs} \sim \lambda_p/4\pi n_p = 43$ nm, which is known as an effective probing depth for the reflected probe beam[27]) according to Eq. (1a), where $n_p = 1.94$ is the refractive index for ZnO at the probe wavelength and ω_p is the probe frequency. Drude formalism allows to calculate the refractive index change by one electron-hole pair, n_{eh}, according to the relation (b),[30] using electron-hole mass m_{eh}^* (m_e^* and m_h^* are the electron and hole effective masses, respectively; ε_0 is the dielectric constant)

$$\mathrm{DR}(t) = \frac{R_0 - R(t)}{R_0} = \frac{-4}{(n_p^2 - 1)} n_{eh}\Delta N(z = d_{obs}, t), \quad (1a)$$

$$n_{eh} = -\frac{e^2}{2n_p\varepsilon_0 m_{eh}^* {\omega_p}^2}, \; \frac{1}{m_{eh}^*} = \left(\frac{1}{m_e^*} + \frac{1}{m_h^*}\right), \quad (1b)$$

$$\mathrm{DE}(t) = \frac{I_{diff}}{I_T} = \left(\frac{\pi n_{eh}}{\lambda_p}\int_0^d \Delta N(z,t)dz\right)^2 \propto \Delta N^2 \exp(-2t/\tau_G),\; 1/\tau_G = 1/\tau_R + 1/\tau_D. \quad (1c)$$

In the LITG measurements, the interference pattern of two pump beams produces the spatially modulated excess carrier density $\Delta N(x, z) = \Delta N_0(1 + \cos(2\pi x/\Lambda)) \times \exp(-\alpha z)$, which acts as a transient diffraction grating (here Λ is the grating period). By monitoring decay of the grating diffraction efficiency DE(t) of the probe beam (see Eq. (1c), here I_{diff} is the diffracted and I_T is the transmitted probe beam intensity), we obtain the grating decay time τ_G, as DE $\propto$ $\exp(-2\,t/\tau_G)$. The LITG is erased due to the recombination of excess carriers (with time τ_R) and their diffusion according to the relationship $(\tau_G)^{-1} = (\tau_R)^{-1} + (\tau_D)^{-1}$, which allows to extract the diffusion coefficient D from the diffusive grating decay time $\tau_D = \Lambda^2/4\pi^2 D$. Average in-depth carrier density is described by $\Delta N = \Delta N_0/2$ relationship.[31]

III. RESULTS AND DISCUSSION

A. PL spectra temperature dependences

The PL spectra of the studied sample are shown in Fig. 2. The spectra revealed features typical for bulk, hydrothermally grown ZnO, namely, the broad band centered at ~2.1 eV, being related to deep-level emission (DLE), including donor–acceptor pair (DAP) transitions (Fig. 2(a)).[32,33] In the low temperature ($T < 150$ K) near band-edge emission spectra (Fig. 2(b)), the observed 3.354 eV peak could be attributed to donor bound exciton (3.357 eV (Ref. 24)) and/or acceptor bound exciton (3.35 eV (Ref. 17)) emission. Exciton binding energy to shallow acceptor (tentatively Li complex) is $E_{bound} \sim 12$ meV (Ref. 17) (for the determined ~240 meV donor it will be $E_{eb} \sim 0.1 E_{imp}$ according to Haynes rule;[17] i.e., very close spectrally). The 3.27 eV line (see Fig. 2(b)) was attributed to other shallow donor-shallow acceptor DAP line. That shallow donor activation energy of ~30–60 meV was determined by Eq. (2), taking into account 120–150 meV shallow acceptor ionisation energy.[17,19] The very shallow donors (30–50 meV) typically are attributed to Zn_i or V_O defects.[32] The deeper ~240 meV donor from Hall measurements can be related to O_{Zn} defects.[34] At higher temperatures ($T > 150$ K), the free exciton LO transitions became dominant in UV range.[35]

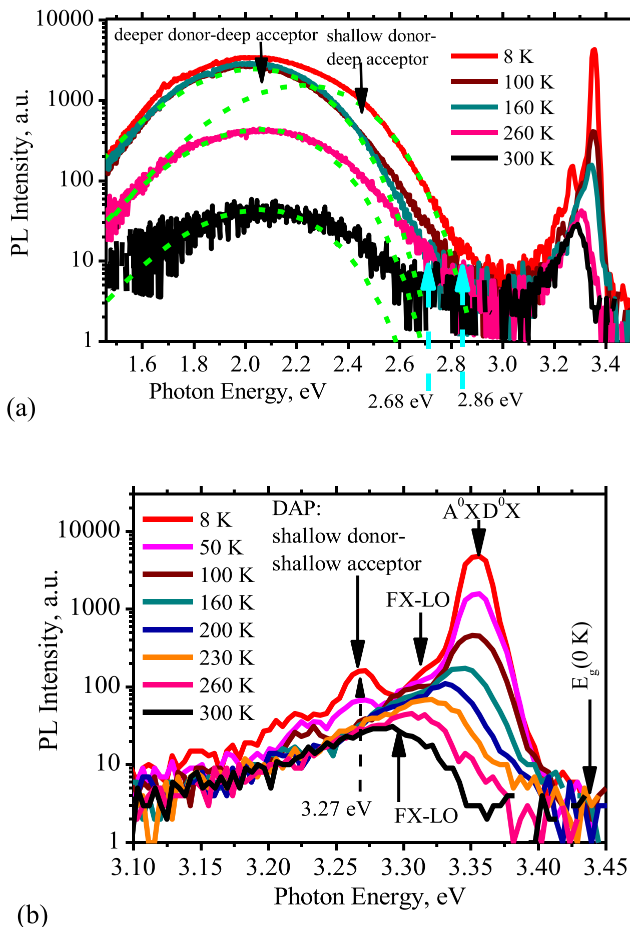

FIG. 2. Evolution of PL spectra in the 8–300 K range in 1.6–3.5 eV VIS interval (a) and in the near band-edge region (b) (part of the (a) spectra). Dashed arrows indicate the ZPL line positions, while dashed lines show ZPL spectra fits, see details in the text.

The near band-edge emission (NBE) efficiency temperature dependence was fitted (Fig. 3) using a fit with free and bound exciton components. The fit equation is $NBE(T) = a_1 f_{ex}(1 - f_{bound}) + a_2 f_{ex} f_{bound}$,[36] where $a_1 = 126$ and $a_2 = 13$ are constants and $f_{ex} = 1/(1 + 70 \times \exp(-E_{ex}/kT))$ is the exciton formation factor, where $E_{ex} = 60$ meV (Ref. 36) is the exciton binding energy and $f_{bound} = 1/(1 + 28 \times \exp(-E_{bound}/kT))$ is the exciton binding factor ($E_{bound} = 12$ meV was used). Assuming that at low temperatures the total radiative PL efficiency is close to unity (Fig. 3), the NBE emission efficiency at low T is only ~10%, while at RT it drops even to ~0.2%. The 60 meV shallow donor-shallow acceptor DAP line and bound exciton peak amplitudes decreased with temperature with similar rate (see Fig. 2(b)), indicating for small shallow donor thermal ionization energy (~12 meV). Latter value is close to that from electrical measurements, ~6 meV. The thermal donor ionisation energy could be lower than that from PL measurements (~30–60 meV) due to impurity band formation[37] as $E_a = E_{a0} - \text{const} \times (N_D)^{1/3}$, where N_d is the donor concentration.

The zero phonon line (ZPL) for DAP transition can be calculated as[33]

$$E_{DAP}(\text{ZPL}) = E_g - (E_A + E_D), \qquad (2)$$

where E_g is the ZnO band-gap ($E_g = 3.437$ eV at 8 K and 3.37 eV at RT[17,35]). E_A and E_D are acceptor and donor activation energies. For DLE transition, only one impurity would be used in Eq. (2), providing rather the same PL band shape.[33] In Fig. 2(a), the ZPL positions were found from fitting of the PL bands (dashed lines), using Poisson distribution function[32] with spectral intensity $E(\text{ZPL} - n\hbar\omega_v) \sim \exp(-S)S^n/n!$ We used Huang-Rhys factor $S = 8.5$ and $\hbar\omega_v = 80$ meV distance between the deep impurity vibrational levels, which are numbered by n. Note that

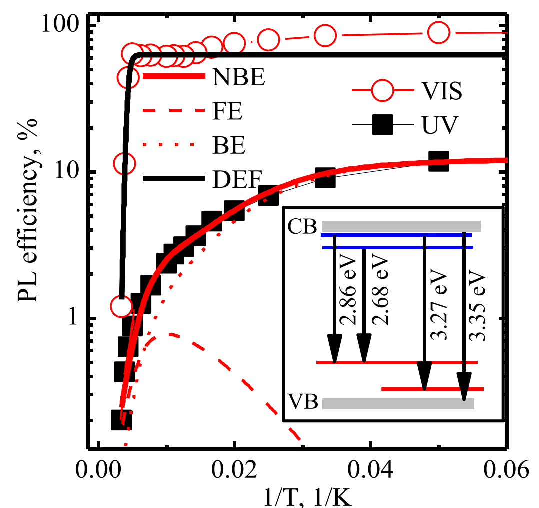

FIG. 3. Evolution of PL efficiency in the visible (VIS) and in ultraviolet (UV) regions. Fits of activated reduction of PL in VIS interval is provided by defect activation fit (DEF), while UV emission was fitted by near band edge emission function (NBE). The latter is composed of bound exciton (BE) and free exciton (FE) emission components. The inset shows a scheme of proposed transitions with corresponding ZPL energies (at 8 K).

the ZPL line intensity is calculated to be ∼700 times weaker than the DAP band peak PL intensity; thus, ZPL position could not be very precisely determined.

In Fig. 2(a), the broad DLE feature in 8–50 K range approximately provided zero phonon line position at 2.86 ± 0.05 eV, while with the increase of temperature (above 100 K), it shifted to lower energy of 2.68 ± 0.05 eV and became slightly narrower. This indicated that at the lowest temperatures, two recombination processes occur, while at higher temperatures, only one should be dominant. At $T < 100$ K, the calculated 2.86 eV DAP ZPL position corresponds probably to shallow donor (∼60 meV) to deep acceptor (with 0.52 ± 0.05 eV energy) recombination process. The deep acceptor is probably Zn vacancy.[1,38] The determined ZPL value well coincides with the zero phonon line 2.859 eV for a ZnO "green" band.[39] In the 8–100 K range, the shallower donor (ZPL at 2.86 eV) is emptied (see the DLE high energy wing reduction, Fig. 2(a)) providing 180 ± 50 meV ZPL redshift and then recombination tentatively prevails through deeper 240 meV donor to 0.52 eV acceptor (2.68 eV ZPL, "yellow band"). The redshift value also indicates that shallow donor should be at ∼60 meV below CB, as if the donor was shallower, the obtained deeper donor energy would differ more from the value from electrical measurements (∼244 meV). Close to room temperature, the fitted DLE spectra are narrower than the experimental ones, as in the higher energy wing the transitions between conduction band and deep acceptor become more evident (2.4–2.7 eV range). This occurs due to donor ionisation. The inset in Fig. 3 shows the scheme of all proposed transitions with corresponding emitted photon energies.

The temperature dependence of PL peak intensity in the visible (VIS) region is provided in Fig. 3. Shallow donor ionization is followed by slight decrease of integral PL intensity above 50 K (see high energy wing in Fig. 2(a)). The thermal activation energy for the deeper donor-deep acceptor DAP band at $T > 100$ K was derived using $DEF(T) = A_{def}/(1 + C_{def} \times \exp(-E_D/kT))$ relation,[17] where $A_{def} = 630$ is the low temperature DAP amplitude, $C_{def} = 9.45 \times 10^8$ is a fitting parameter, while the determined thermal activation energy of $E_D = 430$ meV should correspond to the 0.52 eV deep acceptor. The 90 meV lower thermal deep acceptor activation energy with respect to the optical one (determined from ZPL position) also indicates for impurity band formation ($E_a = E_{a0} - \text{const} \times (N_A)^{1/3}$) due to high acceptor concentration. Using evaluated $\sim 1 \times 10^{19}\,\text{cm}^{-3}$ acceptor concentration, we obtain factor $a = 4 \times 10^{-8}$ cm × eV, which is typical for wide-bandgap semiconductors at high doping densities (for example, in SiC $a = 2.32 \times 10^{-8}$ cm × eV for Al (0.26 eV)[40] and in diamond $a = 6.7 \times 10^{-8}$ cm × eV for boron (0.37 eV)[41]).

Decay of the broad DAP PL band at 300 K was found very slow (∼few microseconds), confirming its attribution to deep defects, while the near-band-edge emission decay was very fast (∼hundreds of picoseconds); latter TRPL decays will be provided elsewhere. To conclude, we clarified the defects present in ZnO and now can transfer to the investigation of their impact on excitation dependent DR and LITG decays in Section III B, i.e., on carrier dynamics.

B. Excitation dependent LITG and DR decays

The grating decay time τ_G for various grating periods ($\Lambda = 0.95$, 1.95, 7.8 μm) was measured and used for the determination of the carrier lifetime τ_R and diffusion coefficient D. In Figs. 4(a) and 4(b), we present kinetics of grating decay at various injection levels for two different temperatures. It was observed that a fast decay component emerges with excitation increase and points out to decreasing with excitation carrier lifetime.

Lifetime measurements by differential reflectivity are shown in Fig. 4(b). Dashed curves in Fig. 4(b) correspond to LITG carrier density decay at the same excitations as in DR case. The LITG decays are slower as monitor an average carrier density, while the DR decay reveals the processes only nearby the surface (DR probes only 43 nm depth, while the LITG signal ∼83 nm, i.e., two times larger). Therefore, the observed DR lifetime is ∼1.4 times shorter as probes twice higher carrier density (note $\tau_R \sim \Delta N^{-0.45}$). Decay times in the DR and LITG kinetics tails are similar as both reveal the low-injection carrier lifetime.

The measured absolute value of DE at RT (2×10^{-4} at 0.2 mJ/cm^2) allowed the estimation of refractive index change per one electron-hole pair $n_{eh} = -(2.0 \pm 0.5) \times 10^{-21}$ cm^3 (according to Eq. (1c)). The latter value coincides with the calculated one, $n_{eh} = \sim -2.0 \times 10^{-21}$ cm^3, taking ZnO electron mass $m_e^* \sim 0.22\ m_0$[26] and $m_h^* = 0.6\ m_0 > m_e^*$.[42] This indicates that electrons mainly contribute to DE signal due to their lower mass (see Eq. (1b)).

The measured absolute value of DR allows the determination of the injected carrier density ΔN near the surface $\Delta N(d_{obs}, t)$. Taking the determined n_{eh} value and absolute DR signal of 0.035 at 0.1 mJ/cm^2, by Eq. (1a), we calculate the value of $\Delta N = \alpha_{ex} I_0/h\nu = 1.2 \times 10^{19}\,\text{cm}^{-3}$. It provides absorption coefficient of $\alpha_{ex} = 1.2 \times 10^5\,\text{cm}^{-1}$ at 355 nm and confirms the reference value of $\alpha_{ex} \sim 1.4 \times 10^5\,\text{cm}^{-1}$.[29]

C. Carrier diffusion coefficient and lifetime temperature dependences by LITG

LITG measurements in the 80–800 K range allowed determination of the recombination rates of free and trapped by defects carriers, as well as the excess carrier diffusion

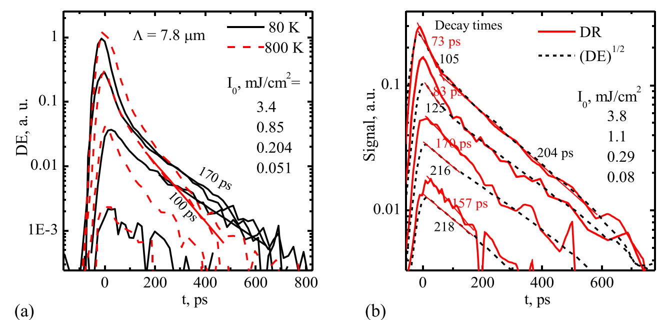

FIG. 4. (a) Kinetics of grating diffraction efficiency at 80 and 800 K for 7.8 μm grating periods. Straight lines indicate exponential fits which provide excess carrier lifetime values of 170 and 100 ps. (b) DR decays at different excitations at 300 K; the dashed curves correspond to carrier density decay $\Delta N(t)$, obtained from LITG decay measurements ($\Delta N \sim (DE)^{1/2}$, see Eq. (1c)).

coefficient D. In turn, the measurements at various excitation intensities provided dependences of τ_R and D on injected carrier density ΔN. In Fig. 5, we present these data for various ΔN values, up to $5 \times 10^{20}\,cm^{-3}$. We note the sublinear decrease of lifetime vs. excitation (with slope ~ -0.45) and the increase of D vs excitation (with slope ~ 0.6). Temperature dependences of D and lifetime values were found useful for analysis of contributing mechanisms. The D increase indicates filling of acceptor centers (similarly as in SiC[43]) and gradual transition from monopolar diffusion to bipolar one at reaching ΔN above $10^{19}\,cm^{-3}$. The lifetime decrease indicates the fast free carrier recombination becoming dominant after saturation of deep acceptor traps.

Rather short lifetimes and very low D values were observed at $T \geq 300\,K$ (Fig. 5(a)). The low D value is a consequence of high density of deep defects (acceptors), which efficiently scatter and capture carriers (holes) at low injections, but after total filling of acceptors by holes at higher excitations the D increases up to $2-3\,cm^2/s$. This value corresponds to bipolar mobility of about $\mu_b = 100 \pm 20\,cm^2/V\,s$ (as derived from Einstein relationship, $D = \mu kT/e$ (Ref. 44)) and the hole mobility of $\mu_h \approx 80 \pm 10\,cm^2/V\,s$ determined by $\mu_b = 2\mu_e\mu_h/(\mu_e + \mu_h)$ relation,[44] using determined electron Hall mobility of $\mu_e = 140\,cm^2/V\,s$. Similar value of hole Hall mobility $\mu_h \approx 90\,cm^2/V\,s$ in Ref. 45 was obtained at $8.3 \times 10^{18}\,cm^{-3}$ p-doping. Decrease of D with the temperature increase (Fig. 5(a)) indicates carrier scattering by acoustic and optical phonon population,[46] as evidenced by the dependence of D on temperature ($D \propto T^{-1.4}$) and the corresponding $\mu \sim T^{-2.4}$ dependence (for comparison, in low-compensated ZnO, the electron mobility follows $\mu \sim T^{-1.9}$ law[34]).

The excitation dependences of D may provide insight into impact of compensating acceptor filling.[43] At low excitations ($\Delta N < 10^{19}\,cm^{-3}$), one type of carriers (holes) should be efficiently captured by deep acceptors at $E_V + 0.52\,eV$. The threshold of sharp D increase at $\sim 1 \times 10^{19}\,cm^{-3}$ (see Fig. 5(a) at $T < 300\,K$) indicates compensating acceptor concentration.[43]

The value is similar to the one obtained from Hall measurements. If dominant acceptors were shallow ($E_a \lesssim 0.2\,eV$), they would be thermally activated at $T > 300\,K$, leading to higher values of D at higher temperatures, and eventually injection-independent D at 800 K would be observed (this case was observed in $\sim 10^{18}\,cm^{-3}$ compensated Al-doped SiC, where Al activation energy was 180 meV (Ref. 43)). Therefore, deep acceptors are more abundant and do not exhibit thermal activation up to 800 K as evidenced by D(T).

On the other hand, the high density of nonradiative traps is confirmed by short 1/e lifetimes of about 200 ps at RT (Fig. 5(b), as determined from LITG kinetics in Fig. 4). This could indicate that carriers recombine through the 0.52 eV acceptors, present in the sample (the closer the trap is located to the midgap, the stronger its impact to the recombination rate[47]). Thus, free electron lifetime decreased as $T^{-\gamma}$ (at low excitations, see Fig. 5(b)), with slope $\gamma \sim -1/2$, following the dependence of thermal velocity of electrons on temperature (as $\tau_{NRe} \sim 1/N_T\sigma_T v_{th}$, where $v_{th} \sim (kT)^{1/2}$ is the thermal velocity of electrons, σ_T is the electrons capture cross section to neutralised (with holes) deep acceptors of density N_T). The lifetimes in decay tails (see Fig. 5(b) at 0.85 mJ/cm^2 excitation Fig. 5) coincide with the lifetime value at low excitation (see Fig. 4(a) at 0.051 mJ/cm^2 Fig. 4), indicating that the initial nonexponential decay at high carrier density is due to excitation-dependent recombination rate. The thermal activation of holes from the acceptor states leads to their capture to fast recombination centers close to midgap position (e.g., V_OZn_i clusters[38]). The subsequent fast electron capture to these mid-gap states impurities will lead to fast component of nonradiative recombination. Thus, at low excitations, the electron lifetime was measured, while at high excitations, the bipolar electron-hole pair lifetime.

Further analysis of $\tau_R(\Delta N)$ dependence (Fig. 5(b)) indicates that excitation dependent recombination rate $1/\tau_R$ in 80–300 K range reveals the impact of another recombination mechanism relevant to bimolecular recombination ($1/\tau_R \propto BN$, where coefficient or radiative recombination B increases at low temperatures, $B \propto T^{-1.5}$). The radiative lifetime vs. T dependence was discriminated from the impact of defects (see dashed line in Fig. 5(b)). Consequently, the B value was calculated using a relationship $1/\tau_R = BN + 1/\tau_{nonrad}$, proving $B = 1.6 \times 10^{-11}\,cm^3/s$ value at RT and its temperature dependence $B(T) = 1.6 \times 10^{-11} \times (T/300\,K)^{-3/2}\,cm^3/s$ (see Fig. 6). The determined value of coefficient B is similar to that in GaN ($2 \times 10^{-11}\,cm^3/s$ at RT[48]) and also decreases as $T^{-1.5}$. This is a consequence of similar electron masses for GaN and ZnO ($m_e^* = 0.19m_0$ and $0.22m_0$, respectively). The determined B(300 K) value provides 60 ns radiative lifetime at $\sim 10^{18}\,cm^{-3}$ carrier density, which jointly with 200 ps nonradiative lifetime provides PL efficiency of $PL_{eff} = 1/\tau_{rad}/(1/\tau_{rad} + 1/\tau_{nonrad}) \sim 0.3\%$, being similar to the determined value from PL measurements at $\sim 10^{18}\,cm^{-3}$ excitations (Fig. 3). The PL efficiency may increase up to 40% at 3.4 mJ/cm^2 excitation (see crossing of dotted and dashed fits of τ_{rad} and τ_{nonrad} in Fig. 5(a)).

At higher temperatures, the recombination rate increased again (see the slope at 0.8 mJ/cm^2 and $T > 300\,K$), probably due to increased free carrier capture to nonradiative traps. In Fig. 5(b), the high injection nonradiative lifetime activation with temperature was fitted with relationship $\tau_{high} = 800/(1 + 50 \times \exp(-E_{tcb}/kT))$ ps, where $E_{tcb} = (70 \pm 10)$ meV

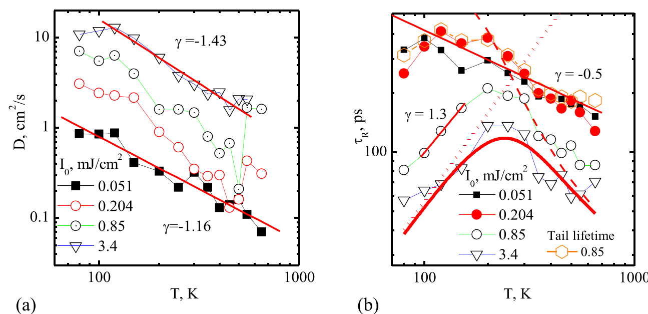

FIG. 5. Diffusion coefficient (a) and 1/e lifetime (b) temperature dependences at different excitation fluences (latter correspond to $\Delta N = 0.55$; 2.2; 9.1; $36 \times 10^{19}\,cm^{-3}$). In (b) the recombination time, determined from decay tail for 0.85 mJ/cm^2 excitation coincides with the lower excitation initial parts (see Fig. 4(a)); fits for lifetime are provided: radiative lifetime for high excitations (dotted line): $\tau_{rad} = 0.056 \times T^{1.5}$ ps; nonradiative free carrier pair lifetime (dashed line): $\tau_{high} = 800/(1 + 50 \times \exp(-70\,meV/kT))$ ps; the lower solid line indicates total recombination rate $1/\tau = 1/\tau_{high} + 1/\tau_{rad}$.

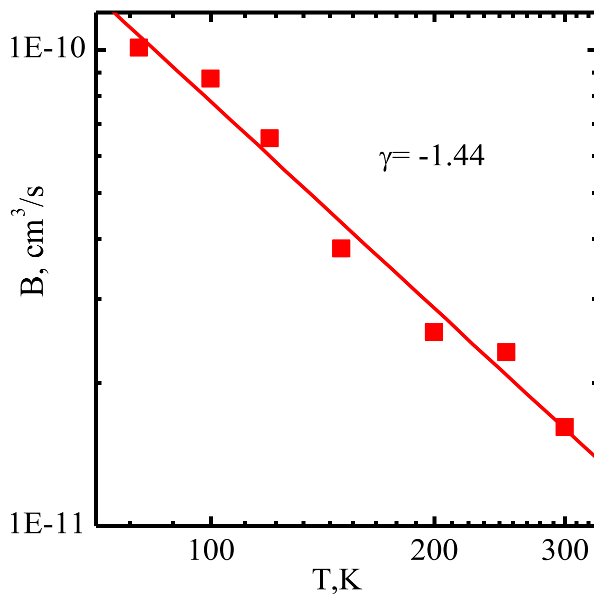

FIG. 6. Bimolecular recombination coefficient temperature dependence, calculated using low and high (0.85 mJ/cm^2) excitation 1/e decay times.

can be attributed to free carrier capture barrier to nonradiative traps.[47]

IV. SUMMARY

Optical studies of bulk hydrothermal n-type ZnO revealed bound exciton and deep level related transitions between donor states (at 60 and 240 meV) and deep acceptor states (at 0.52 eV above the valence band). Decrease of DLE PL emission band intensity with temperature corresponds to the deep acceptor thermal activation energy of $E_a = 440$ meV, being reduced due to high unintentional doping. LITG measurements allowed determination of carrier lifetime and diffusion coefficient dependences on injection and temperature. Low excitation lifetime decreased with temperature as $T^{-0.5}$, indicating electron recombination through deep defects. Low value of diffusion coefficient was observed at excitations below the fixed excess carrier value, and this feature pointed out to the presence of deep acceptors with the density of $\sim 10^{19}$ cm^{-3}, i.e., by order of magnitude larger than that of Li. Electron and hole mobilities of 140 and ~ 80 cm^2/V s at RT were determined, combining LITG and Hall measurements. At high injections and $T < 300$ K, the bimolecular recombination was discriminated from the defect-governed recombination. The bimolecular coefficient followed $1.6 \times 10^{-11} \times (T/300\,K)^{-3/2}$ cm^3/s trend. At $T > 300$ K, nonradiative recombination prevailed and lifetime decreased with activation energy of 70 meV, revealing the possible presence of a barrier for the carrier capture to nonradiative traps.

ACKNOWLEDGMENTS

The work was supported by Latvian National Research Programme in Materials Science (IMIS2), (2014-2017). Latvian Science Council Grant No 402/2012. P.Š. acknowledges support from Lithuanian Academy of Science via the Young Scientists Scholarship. We also acknowledge Dr. L. Trinkler for manuscript reading and valuable comments.

[1]A. Janotti and C. G. Van de Walle, Rep. Prog. Phys. **72**, 126501 (2009).
[2]M. H. Huang, S. Mao, H. Feick, H. Yan, Y. Wu, H. Kind, E. Weber, R. Russo, and P. Yang, Science **292**, 1897 (2001).
[3]D. M. Bagnall, Y. F. Chen, Z. Zhu, T. Yao, S. Koyama, M. Y. Shen, and T. Goto, Appl. Phys. Lett. **70**, 2230 (1997).
[4]L. N. Protasova, E. V. Rebrov, K. L. Choy, S. Y. Pung, V. Engels, M. Cabaj, A. E. H. Wheatley, and J. C. Schouten, Catal. Sci. Technol. **1**, 768 (2011).
[5]T. Pompe, V. Srikant, and D. R. Clarke, Appl. Phys. Lett. **69**, 4065 (1996).
[6]Y. Zhang, K. Yu, D. Jiang, Z. Zhu, H. Geng, and L. Luo, Appl. Surf. Sci. **242**, 212 (2005).
[7]M. Matsui, Y. Hashimoto, K. Funabiki, J.-Y. Jin, T. Yoshida, and H. Minoura, Synth. Met. **148**, 147 (2005).
[8]S. Larcheri, C. Armellini, F. Rocca, A. Kuzmin, R. Kalendarev, G. Dalba, R. Graziola, J. Purans, D. Pailharey, and F. Jandard, Superlattices Microstruct. **39**, 267 (2006).
[9]H. L. Zhou, S. J. Chua, S. Y. Chow, H. Pan, Y. W. Zhu, Y. P. Feng, L. S. Wang, K. Y. Zang, W. Liu, and S. Tripathy, J. Phys. Condens. Matter **19**, 356203 (2007).
[10]D. C. Look, D. C. Reynolds, J. R. Sizelove, R. L. Jones, C. W. Litton, G. Cantwell, and W. C. Harsch, Solid State Commun. **105**, 399 (1998).
[11]D. C. Reynolds, C. W. Litton, D. C. Look, J. E. Hoelscher, B. Claflin, T. C. Collins, J. Nause, and B. Nemeth, J. Appl. Phys. **95**, 4802 (2004).
[12]K. Maeda, M. Sato, I. Niikura, and T. Fukuda, Semicond. Sci. Technol. **20**, S49 (2005).
[13]J. Mass, M. Avella, J. Jiménez, M. Callahan, E. Grant, K. Rakes, D. Bliss, and B. Wang, Appl. Phys. A **88**, 95 (2007).
[14]See http://crystalbase.co.jp/index/a/zno.html for Crystal Base Co.,Ltd. web page.
[15]K. M. Johansen, H. Haug, Ø. Prytz, P. T. Neuvonen, K. E. Knutsen, L. Vines, E. V. Monakhov, A. Y. Kuznetsov, and B. G. Svensson, J. Electron. Mater. **40**, 429 (2010).
[16]M. Gabás, A. Landa-Cánovas, J. Luis Costa-Krämer, F. Agulló-Rueda, A. R. González-Elipe, P. Díaz-Carrasco, J. Hernández-Moro, I. Lorite, P. Herrero, P. Castillero, A. Barranco, and J. Ramón Ramos-Barrado, J. Appl. Phys. **113**, 163709 (2013).
[17]S. H. Lee, J. S. Lee, W. B. Ko, J. I. Sohn, S. N. Cha, J. M. Kim, Y. J. Park, and J. P. Hong, Appl. Phys. Express **5**, 95002 (2012).
[18]Y. J. Zeng, Z. Z. Ye, W. Z. Xu, D. Y. Li, J. G. Lu, L. P. Zhu, and B. H. Zhao, Appl. Phys. Lett. **88**, 062107 (2006).
[19]C. Rauch, W. Gehlhoff, M. R. Wagner, E. Malguth, G. Callsen, R. Kirste, B. Salameh, A. Hoffmann, S. Polarz, Y. Aksu, and M. Driess, J. Appl. Phys. **107**, 024311 (2010).
[20]M. G. Wardle, J. P. Goss, and P. R. Briddon, Phys. Rev. B **71**, 155205 (2005).
[21]A. Carvalho, A. Alkauskas, A. Pasquarello, A. K. Tagantsev, and N. Setter, Phys. B Condens. Matter **404**, 4797 (2009).
[22]Y. Y. Sun, T. A. Abtew, P. Zhang, and S. B. Zhang, Phys. Rev. B **90**, 165301 (2014).
[23]M. D. McCluskey, C. D. Corolewski, J. Lv, M. C. Tarun, S. T. Teklemichael, E. D. Walter, M. G. Norton, K. W. Harrison, and S. Ha, J. Appl. Phys. **117**, 112802 (2015).
[24]S. L. Chen, W. M. Chen, and I. A. Buyanova, Appl. Phys. Lett. **102**, 121103 (2013).
[25]J. Pernot, W. Zawadzki, S. Contreras, J. L. Robert, E. Neyret, and L. Di Cioccio, J. Appl. Phys. **90**, 1869 (2001).
[26]*Oxide and Nitride Semiconductors*, edited by T. Yao and S.-K. Hong (Springer, Berlin/Heidelberg, 2009).
[27]A. Sabbah and D. Riffe, Phys. Rev. B **66**, 165217 (2002).
[28]K. Jarasiunas, R. Aleksiejunas, T. Malinauskas, V. Gudelis, T. Tamulevicius, S. Tamulevicius, A. Guobiene, A. Usikov, V. Dmitriev, and H. J. Gerritsen, Rev. Sci. Instrum. **78**, 033901 (2007).
[29]R. C. Rai, M. Guminiak, S. Wilser, B. Cai, and M. L. Nakarmi, J. Appl. Phys. **111**, 073511 (2012).
[30]G. R. Fowles, *Introduction to Modern Optics* (Rinehart and Winston, New York, 1975).
[31]P. B. Klein, R. Myers-Ward, K.-K. Lew, B. L. VanMil, C. R. Eddy, D. K. Gaskill, A. Shrivastava, and T. S. Sudarshan, J. Appl. Phys. **108**, 033713 (2010).
[32]U. Özgür, Y. I. Alivov, C. Liu, A. Teke, M. A. Reshchikov, S. Doğan, V. Avrutin, S.-J. Cho, and H. Morkoç, J. Appl. Phys. **98**, 041301 (2005).
[33]M. A. Reshchikov and H. Morkoç, J. Appl. Phys. **97**, 061301 (2005).
[34]A. Tsukazaki, A. Ohtomo, and M. Kawasaki, Appl. Phys. Lett. **88**, 152106 (2006).
[35]L. Wang and N. C. Giles, J. Appl. Phys. **94**, 973 (2003).
[36]B. K. Meyer, H. Alves, D. M. Hofmann, W. Kriegseis, D. Forster, F. Bertram, J. Christen, A. Hoffmann, M. Straßburg, M. Dworzak, U. Haboeck, and A. V. Rodina, Phys. Status Solidi **241**, 231 (2004).

[37]W. Gajewski, P. Achatz, O. Williams, K. Haenen, E. Bustarret, M. Stutzmann, and J. Garrido, Phys. Rev. B **79**, 045206 (2009).
[38]M. Willander, O. Nur, J. R. Sadaf, M. I. Qadir, S. Zaman, A. Zainelabdin, N. Bano, and I. Hussain, Materials (Basel) **3**, 2643 (2010).
[39]M. Grundmann, *The Physics of Semiconductors*, 2nd ed. (Springer, Berlin/Heidelberg, 2010).
[40]P. Achatz, J. Pernot, C. Marcenat, J. Kacmarcik, G. Ferro, and E. Bustarret, Appl. Phys. Lett. **92**, 072103 (2008).
[41]I. Stenger, M.-A. Pinault-Thaury, T. Kociniewski, A. Lusson, E. Chikoidze, F. Jomard, Y. Dumont, J. Chevallier, and J. Barjon, J. Appl. Phys. **114**, 073711 (2013).
[42]K. Hümmer, Phys. Status Solidi **56**, 249 (1973).
[43]G. Liaugaudas, P. Ščajev, and K. Jarašiūnas, Semicond. Sci. Technol. **29**, 015004 (2014).
[44]J. F. Schetzina and J. P. McKelvey, Phys. Rev. B **2**, 1869 (1970).
[45]H. B. Ye, J. F. Kong, W. Z. Shen, J. L. Zhao, and X. M. Li, Appl. Phys. Lett. **90**, 102115 (2007).
[46]P. Wagner and R. Helbig, J. Phys. Chem. Solids **35**, 327 (1974).
[47]B. K. Ridley, *Quantum Processes in Semiconductors* (OUP, Oxford, 1999).
[48]T. Malinauskas, K. Jarašiūnas, R. Aleksiejunas, D. Gogova, B. Monemar, B. Beaumont, and P. Gibart, Phys. Status Solidi **243**, 1426 (2006).